Carbon-doped TiO$_2$ nanoparticles wrapped with nanographene as a high performance photocatalyst for phenol degradation under visible light irradiation

Sungju Yu, Hyeong Jin Yun, Yong Hwa Kim, Jongheop Yi[*]

World Class University Program of Chemical Convergence for Energy & Environment, School of Chemical and Biological Engineering, Institute of Chemical Processes, Seoul National University, Seoul 151-742, Republic of Korea

A B S T R A C T

With a view to developing photocatalytic applications under irradiation by visible light, many efforts have been devoted to modifying band structure of TiO$_2$ by doping with metal and non-metal ions. Although doping techniques promote the absorption of visible light, it is usually accompanied by the formation of defect sites. Consequently, photocatalytic activity cannot be improved when the concentration of defects is high. Here we wrapped each of carbon-doped TiO$_2$ (C-TiO$_2$) nanoparticles (NPs) with nano-sized graphene (nGR) for use as a high performance material for the phenol degradation and quantified the enhanced photoelectrochemical properties compared to bare C-TiO$_2$ NPs and C-TiO$_2$ NPs distributed on micro-sized graphene (C-TiO$_2$/μGR). C-TiO$_2$ NPs wrapped with nGR (nGR@C-TiO$_2$) showed outstanding oxidizing power than those of bare C-TiO$_2$ NPs, C-TiO$_2$/μGR and commercial TiO$_2$ (P25). It is proven that nGR@C-TiO$_2$ possesses the low interfacial charge-transfer resistance between C-TiO$_2$ and reactant. As a result, prolonged lifetime of photogenerated charges over the C-TiO$_2$ NPs caused the formation of the larger amount of hydroxyl radicals (•OH) with strong oxidizing power for the phenol degradation.

© 2013 Elsevier B.V. All rights reserved.

1. Introduction

The TiO$_2$–graphene composites have been investigated for the various applications, including the degradation of organic pollutants, production of H$_2$ *via* water splitting, reduction of CO$_2$ for solar fuel production, and so on [1–8]. These research indicate that the contact of TiO$_2$ with graphene is known to improve the photocatalytic performance compared to the bare TiO$_2$ due to the increased adsorption of pollutants, extended light absorption range and enhanced charge separation [6–8]. Graphene also served as an acceptor of the photogenerated electrons and reduced the charge recombination because the photogenerated electrons of TiO$_2$ are transferred from the conduction band to graphene *via* a percolation mechanism [8,9]. In particular, it is reported that TiO$_2$ particles wrapped with graphene sheet reduced the probability of charge recombination in the degradation of methylene blue and hydrogen generation *via* water splitting compared to TiO$_2$ particles distributed on graphene sheet [1,2]. However, these results showed relatively low efficiency under the visible light that TiO$_2$ could utilize no more than 5% of the total solar energy impinging on the surface of the earth due to its wide band-gap energy (E_g, 3–3.2 eV) [10].

One of the most effective ways to develop visible light responsive photocatalysts is to create impurity levels in the forbidden band *via* a doping technique. Metal and non-metal dopants, however, have been considered as an active center of charge recombination. In addition, they can not only induce the formation of vacancy sites, but work as an active center of charge recombination. It is the reason why most of impurity-doped semiconductors suffer from their lower activities. This phenomenon have been supported by computational results as well as experimental studies [11–15]. Thus, it is a challenge of great importance to design an efficient visible light responsive nano-photocatalytic material to reduce the charge recombination.

Here, we introduce a facile method to wrap each of carbon-doped TiO$_2$ (C-TiO$_2$) nanoparticles (NPs) with nano-sized graphene (nGR) and quantify the enhanced photoelectrochemical properties compared to bare C-TiO$_2$ NPs and C-TiO$_2$ NPs distributed on micro-sized graphene (μGR). It has been reported the synthesis of C-TiO$_2$ NPs by wet chemistry [16]. This method allows one to form uniform sized C-TiO$_2$ NPs as well as dope a high amount of carbon. Nano-sized graphene oxide (nGO) was prepared by a two-step oxidation of graphite, which were characterized by AFM [2,17]. It showed that the thickness and size of nGO vary in the range of 0.8–2.0 nm and 30–40 nm, respectively (Fig. S1).

* Corresponding author. Tel.: +82 2 880 7438.
  E-mail address: jyi@snu.ac.kr (J. Yi).

2. Experimental

2.1. Catalyst preparation

2.1.1. Synthesis of micro-sized graphene and nano-sized graphene

Micro-sized graphene oxide (μGO) was synthesized by the improved method, following a procedure reported in the literature [18]. Graphite flakes (Sigma–Aldrich, 1.5 g) was added to a mixture of concentrated H_2SO_4 (≥95%, Samchun, 180 mL)/H_3PO_4 (≥85%, Samchun, 20 mL), and KMnO4 (≥99.3%, Samchun, 9.0 g) was then slowly added with vigorous stirring for 12 h at 45 °C. The mixture was cooled to room temperature, and 200 mL of a H_2O_2 solution (190 mL of water + 10 mL of 30 wt% H_2O_2) was then slowly added. The solution stirred for 1 h. The resultant solution was ultrasonicated for 30 min, and then centrifuged. The precipitate was then washed with water, HCl (35–37%, Samchun), and ethanol repeatedly. The washed precipitate was coagulated by adding ether (≥99%, Sigma–Aldrich). Finally, yellow powder was obtained by vacuum-drying overnight at room temperature.

nGO was synthesized by a two-step oxidation of graphite [2]. The graphite oxide (0.05 g) obtained by a procedure described above was added to a concentrated H_2SO_4 solution (≥95%, Samchun, 50 mL), and KMnO4 (≥99.3%, Samchun, 0.15 g) was then slowly added with vigorous stirring for 3 h at 45 °C. The mixture was cooled to room temperature, and 100 mL of a H_2O_2 solution (95 mL of water + 5 mL of 30 wt% H_2O_2) was then slowly added. The solution stirred over 1 h. The resultant solution was ultrasonicated for 30 min, and then centrifuged. The precipitate was then washed with water, HCl (35–37%, Samchun), and ethanol. The washed precipitate was suspended in a 40 mL of deionized water (DI water).

2.1.2. Synthesis of carbon-doped TiO_2 nanoparticles

C-TiO_2 NPs were synthesized by a gel-hydrothermal method [16]. A total of 0.2 mol of titanium tetraisopropoxide (≥98%, Advanced Materials Institute Co. Ltd.) was added to 0.4 mol of triethanolamine (≥98%, Sigma–Aldrich). DI water was then added to give 400 mL of an aqueous solution. This solution (30 mL) was mixed with 0.02 M oleic acid solution (Samchun, 30 mL). The pH of medium solution was controlled to pH 8 by adding nitric acid (≥60%, Samchun). This mixture was placed in a Teflon-lined autoclave and heated at 100 °C for 12 h to form a Ti(OH)$_4$ gel, which was then heated at 250 °C for 48 h, to give brown-colored precipitates. The organic residue located on the surface of C-TiO_2 NPs was completely removed by heating at 320 °C for 8 h under an air atmosphere. Anatase TiO_2 NPs were prepared a procedure described above, except that a calcination temperature of 450 °C was used.

2.1.3. Synthesis of carbon-doped TiO_2 nanoparticles wrapped with nano-sized graphene

To wrap the surface of C-TiO_2 NPs with nGR, C-TiO_2 NPs (0.7 g) were first dispersed in a solution of DI water (60 mL) and ethanol (30 mL) by sonication for 30 min. Different amounts (0, 0.05, 0.1, 0.5, 1.0 wt% of C-TiO_2) of negatively charged nGO suspension (0.05 g/mL) was added into the suspension under vigorous stirring at pH 3.5. The resulting suspension was transferred to a Teflon-sealed autoclave and maintained at 120 °C for 24 h. The resulting composite was centrifuged, and washed with 1 M HCl aqueous solution and DI water. C-TiO_2/μGR was prepared a procedure described above, except that a μGO was used instead of nGO.

2.2. Catalyst characterization

Morphology and microstructure were investigated by high-resolution transmission electron microscopy (HR-TEM, JEM 3010-JEOL, 300 kV) and X-ray diffraction (XRD, D/max-2500/PC-Rigaku) with Cu Kα radiation (λ = 0.154 nm) as the incident beam at 50 kV and 100 mA. The optical absorbance spectra were obtained by ultraviolet diffuse reflectance spectroscopy (UV-DRS, V670-Jasco), with $BaSO_4$ as the reference. The reduction state of nGO on the surface of C-TiO_2 NPs was analyzed using X-ray photoelectron spectroscopy (XPS, Thermo). The binding energy determined by XPS was corrected with reference to the C 1s peak (284.5 eV) for each sample. Raman results were acquired by using Raman Spectrometer (T64000-HORIABA Jobin Yvon), and the samples were excited by using the Ar laser (514 nm).

Electrochemical impedance spectroscopy (EIS) measurements were performed on the computer-controlled potentiostat (Ivium-Stat, Ivium) using standard three-electrode cell. Powder-typed samples were immobilized on the ITO glass using a doctor blade (0.5 cm × 0.5 cm). Platinum was used as the counter electrode, and saturated Ag/AgCl electrode was used as the reference electrode in a 0.1 M $NaClO_4$ solution under visible light irradiation (λ ≥ 420 nm). EIS experiments were conducted with an applied potential of 1.0 V under an ac perturbation signal of 10 mV over the frequency range of 1 MHz to 3 mHz. The temperature was maintained at 20 °C by circulating water through an external temperature control device during the EIS experiments. The impedance spectra were interpreted using commercial software ZMAN 2.2.

2.3. Characterization of photocatalytic activities

Time-resolved photoluminescence (TRPL) measurements decay curves were obtained via time-correlated single photon counting methods using Fluo-Time 200 instrument (Picoquant, Germany). A 405 nm pulsed diode laser (pulse energy = 10 pJ; FWHM < 54 ps) with the repetition rate of 80 MHz was used as an excitation source. The signals were collected at the excitonic emission of rhodamine B (RhB, Sigma, for fluorescence, λ_{em} = 580 nm). The temperature was maintained at 20 °C by circulating water through an external temperature control device during the TRPL measurements.

The amount of hydroxyl radicals (•OH) generated by the photocatalysis were measured by a colorimetric probe-assisted spectrometric method under visible light irradiation (λ ≥ 420 nm). The photocatalysts (0.03 g) were suspended in 20 μM p-nitrosodimethylaniline (RNO, Sigma–Aldrich) solution (20 mL) maintained pH 7.1 by 5 mM phosphate buffer solution. The reaction temperature was maintained at 20 °C by circulating water through an external temperature control device. The concentration of the RNO was determined by UV–vis spectroscopy. •OH generation, as a result of the degradation of RNO, was estimated at 440 nm.

The photocatalytic activities of the prepared samples were evaluated by the photodegradation of phenol under visible light irradiation by a 300 W Xe lamp with a 420 nm cut-off filter because phenol is one of the most non-degradable organic pollutants. The photocatalysts (0.15 g) were suspended in an aqueous solution of 10 ppm phenol (100 mL). Before illumination, the solution was stirred for 1 h in the dark in order for adsorption–desorption equilibrium to be reached between the photocatalyst and phenol. The reaction temperature was maintained at 20 °C by circulating water through an external temperature control device. The suspension (1 mL) was sampled and filtered using a disposable syringe filter at 1 h intervals. The concentration of phenol was determined by high performance liquid chromatography (HPLC, YL9100-Young Lin Instrument). Target compounds were quantified using HPLC on a 150 mm × 4.6 mm Zorbax Eclipse XDB-C18 column connected to a UV detector (YL9120-Young Lin Instrument). The detection wavelength was set at 210 nm. The mobile phase was a 50% aqueous solution of acetonitrile, pumped at a flow rate of 1 mL/min. A total of 20 μL of sample was injected into the column.
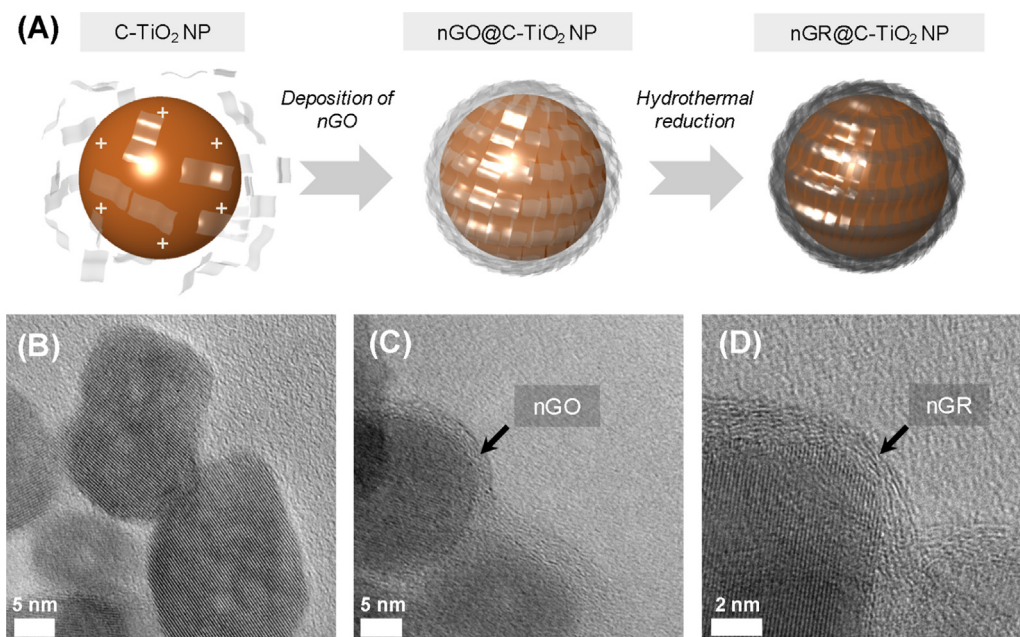
Fig. 1. (A) Synthesis scheme of the preparation procedure of carbon-doped TiO$_2$ nanoparticles (C-TiO$_2$ NPs) wrapped with nano-sized graphene (nGR). First step indicates the surface state of C-TiO$_2$ NPs with weakly positive charge in aqueous suspension (pH 3.5). Second, C-TiO$_2$ NPs are wrapped with the negatively charged nano-sized graphene oxide (nGO). Third, nGO is reduced to nGR by a hydrothermal treatment using ethanol–water as solvent. High-resolution TEM images show (B) C-TiO$_2$ NPs, (C) C-TiO$_2$ NPs wrapped with nGO (nGO@C-TiO$_2$), (D) C-TiO$_2$ wrapped with nGR (nGR@C-TiO$_2$).

3. Results and discussion

3.1. Catalyst characterization

In the previous study, we reported on the facile synthesis of a visible light responsive C-TiO$_2$ NPs. The findings that carbon is clearly incorporated into the TiO$_2$ framework were demonstrated by XRD, TPO, XANES, and EXAFS [19]. In particular, Ti K-edge XANES spectra of C-TiO$_2$ NPs indicated the Ti atom in C-TiO$_2$ is located in a sixfold coordinated sites, which is typical for anatase-structured TiO$_2$ [20,21]. It means that carbon dopant is substitutionally incorporated by replacing oxygen atom in the TiO$_2$

framework. Furthermore, EXAFS spectra of the C-TiO$_2$ NPs showed that the interatomic distances of Ti–O and Ti–Ti in the C-TiO$_2$ NPs become longer than those of pure anatase-structured TiO$_2$ due to the longer bonding length of Ti–C [22], while the sixfold coordination environment around Ti atoms remained unchanged. The incorporation of carbon into the TiO$_2$ framework should have an effect on the binding energy (BE) of O 1s. Fig. S2 shows the BE of O 1s of bare anatase-structured TiO$_2$ and C-TiO$_2$. The BE at 529.8 eV (peak 1) is attributed to the regular lattice oxygen. The BE peaks centered at 531.6 eV (peak 2) and 533.0 eV (peak 3) is attributed to the oxygen in carbonate. The peak 2 and 3 for C-TiO$_2$ are shifted to lower BE (black arrow), which might be related with the creation of oxygen vacancies as a result of the carbon doping [23,24]. The peak shift can be regarded as indirect evidence of successful carbon doping into TiO$_2$ crystal framework.
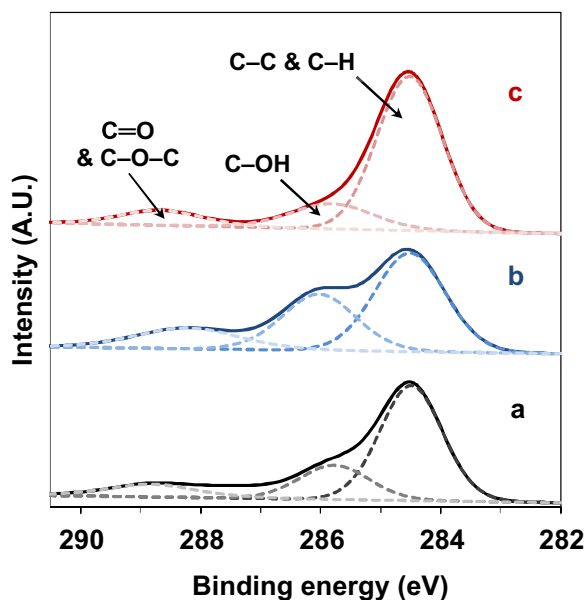
Fig. 2. C 1s XPS spectra of (a) bare C-TiO$_2$ NPs, (b) 0.1% nGO@C-TiO$_2$ and (c) 0.1% nGR@C-TiO$_2$.
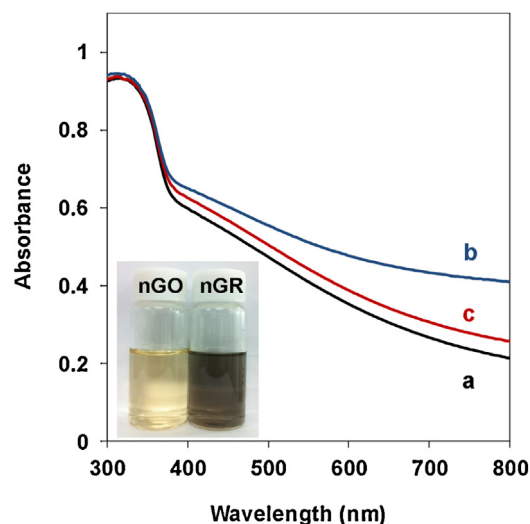
Fig. 3. UV–vis spectra of (a) bare C-TiO$_2$ NPs, (b) C-TiO$_2$/0.1% μGR and (c) 0.1% nGR@C-TiO$_2$. The inset picture shows the aqueous suspensions of nGO and nGR.
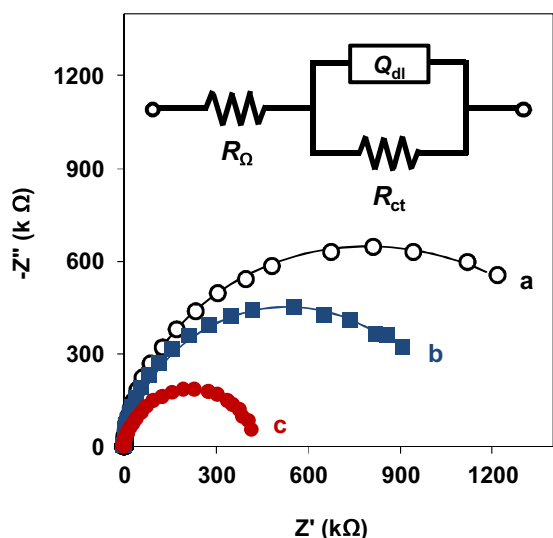
Fig. 4. Nyquist plots of (a) bare C-TiO$_2$ NPs, (b) C-TiO$_2$/0.1% μGR and (c) 0.1% nGR@C-TiO$_2$. The EIS measurements were performed in aqueous electrolyte of 0.1 M NaClO$_4$ under visible light irradiation ($\lambda \geq 420$ nm). Inset figure shows an equivalent circuit which described the electrical response of electrode. R_Ω: bulk electrolyte resistance; Q_{dl}: electrochemical double-layer capacitance; R_{ct}: charge-transfer resistance.

C-TiO$_2$ NPs wrapped with nGR (nGR@C-TiO$_2$) were prepared by utilizing the differences in surface charge between the C-TiO$_2$ and nGO, followed by a hydrothermal treatment (Fig. 1A). The deposition and the reduction of nGO onto the C-TiO$_2$ NPs were simultaneously achieved using this procedure [7,8]. The HR-TEM images in Fig. 1B provide information on their size (diameter = 25.1 ± 4.5 nm), shape and lattice arrays of interplanar distances corresponding to [1 0 1], indicating a typical anatase structure. As shown in Fig. 1C, the positively charged C-TiO$_2$ NPs were wrapped with the negatively charged nGO in aqueous dispersions (pH 3.5) where the amount of nGO was adjusted by controlling the initial amount of nGO used (0, 0.05, 0.1, 0.5, 1.0 wt%). The final product, nGR@C-TiO$_2$, was obtained after the hydrothermal reduction in ethanol-water solvent (Fig. 1D). For comparison, C-TiO$_2$ NPs distributed on μGR (C-TiO$_2$/μGR) were prepared by a procedure described above, except that a μGO (0, 0.1, 0.3, 0.5, 1.0 wt%) was used instead of nGO. The HR-TEM images of C-TiO$_2$/μGR were shown in Fig. S3.

The amount of oxygen-containing functional groups for nGR on the surface of C-TiO$_2$ NPs was significantly lower than that for nGO, as evidenced by a comparison of the C 1s XPS spectra (Fig. 2) [2,6]. This result has a good agreement with the inset picture shown in Fig. 3. The nGO suspension in water appears bright yellow, which indicates that oxygen-containing functional groups on the surface of nGO are abundant [6,25]. In addition, it was investigated by Raman spectroscopy that structural changes of the nGO/nGR and μGO/μGR by the appearance of G and D bands, which are located at around 1600 and 1352 cm^{-1} respectively (Fig. S4A and B). The intensity ratio of the D and G bands (I_D/I_G) is a measure of the relative concentration of local defects or disorders (particularly sp^3 hybridized defects) compared to the sp^2 hybridized graphene domains [5,6]. The I_D/I_G ratio was 0.98 for nGR, which is lower than 1.10 for nGO. The I_D/I_G ratio was 0.99 for μGR, which is lower than 1.07 for μGO. This indicates that the density of defects for nGR and μGR was lower than that for nGO and μGO after the hydrothermal reduction. In both cases of nGR@C-TiO$_2$ and C-TiO$_2$/μGR, their microstructures were not changed with their anatase structure and maintained regardless of the amount of nGR and μGR (Fig. S5A and B). There was no typical diffraction peak indicating graphene around 25° in the XRD patterns due to the low

Table 1
Parameters extracted from fitted results of EIS spectra for each sample.[a]

| Sample	R_Ω (Ω)	Q_0 (Ssec^n)	R_{ct} (MΩ)
(a) C-TiO$_2$	67.686	1.076×10^{-5}	1.583
(b) C-TiO$_2$/0.1% μGR	62.212	1.394×10^{-5}	1.063
(c) 0.1% nGR@C-TiO$_2$	44.880	1.426×10^{-5}	0.436

[a] Calculated using the software ZMAN 2.2.

concentration of graphene and relatively strong diffraction intensity of anatase structure. The optical properties of each sample were characterized by UV-DRS (Fig. 3). As reported in another literature, bare C-TiO$_2$ NPs showed a E_g of about 2.5 eV [26,27]. C-TiO$_2$ NPs wrapped with 0.1 wt% nGR (0.1% nGR@C-TiO$_2$) resulted in reduced E_g to 2.3 eV. In addition, a broad absorption of 0.1% nGR@C-TiO$_2$ over the entire visible range increased, compared to that of bare C-TiO$_2$ NPs due to the presence of nGR. It should be noted that the visible light absorption of nGR@C-TiO$_2$ was lower than that for C-TiO$_2$/μGR with the same amount of graphene. The larger amount of nGR and μGR is present, the more photons are absorbed in a broad wavelength (Fig. S6A and B).

In order to characterize an interfacial reaction between photocatalyst and reactant, electrochemical impedance spectroscopy (EIS) was performed under the irradiation of visible light ($\lambda \geq 420$ nm) and presented as Nyquist plots (Fig. 4). The equivalent circuit for the photoelectrochemical reaction was designed with a serial combination of bulk electrolyte resistance (R_Ω) and electrochemical interfacial reaction impedance represented as a parallel combination of the electrochemical double-layer capacitance (Q_{dl}) and charge-transfer resistance (R_{ct}) as shown in inset of Fig. 4. In this circuit, the constant phase element (CPE) can replace the Q_{dl} at the electrode-electrolyte interface. The impedance of CPE (Z_{CPE}) is given as follows [27],

$$Z_{CPE} = \frac{1}{Q_0(jw)^n} \tag{1}$$

where Q_0 is the admittance magnitude of CPE and n is the exponent related to the phase angle φ by $\varphi = n(\pi/2)$. In the present work, the value of n is fixed at 0.9. The radius of semicircles for both 0.1% nGR@C-TiO$_2$ and C-TiO$_2$/0.1% μGR were much smaller than that of bare C-TiO$_2$ NPs, which means that the presence of
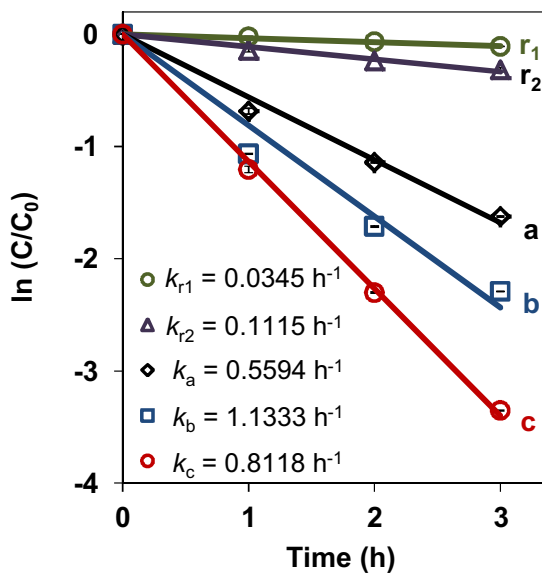
Fig. 5. Photocatalytic decomposition of 10 ppm phenol under visible light irradiation ($\lambda \geq 420$ nm) by (a) bare C-TiO$_2$ NPs, (b) C-TiO$_2$/0.1% μGR, (c) 0.1% nGR@C-TiO$_2$ and (r$_1$) anatase TiO$_2$ NPs, (r$_2$) Degussa P25 as references.

Table 2

Kinetic analysis of emission decay for RhB in the presence of bare C-TiO$_2$ NPs, C-TiO$_2$/0.1% µGR and 0.1% nGR@C-TiO$_2$.

Entry	A_1	τ_1 (ns)	A_2	τ_2 (ns)	k_{et} (s^{-1})	χ^2
RhB	17,746.4	1.696	–	–	–	1.042
RhB + C-TiO$_2$	17,490.0	1.673	246.0	8.598	8.04×10^6	1.023
RhB + C-TiO$_2$/0.1% µGR	17,694.0	1.654	199.3	4.849	1.50×10^7	1.038
RhB + 0.1% nGR@C-TiO$_2$	17,936.0	1.642	74.8	6.453	1.94×10^7	0.989

graphene leads to the remarkable increase in the charge-transfer rate. The extracted parameters from circuit elements are summarized in Table 1. It is found that the R_{ct} of 0.1% nGR@C-TiO$_2$ is much less than any other samples due to the increase in the contact area between C-TiO$_2$ and graphene. Thus, this significantly reduces the probability of charge recombination [8,28].

3.2. Characterization of photocatalytic activities under visible light

To investigate photocatalytic performances under visible light, we carried out the photocatalytic oxidative decomposition of phenol under irradiation by visible light ($\lambda \geq 420$ nm). As shown in Fig. 5, the rate constant for phenol photodegradation (k_{rxn}) of 0.1% nGR@C-TiO$_2$ was 1.1333 h^{-1}, which is twice faster than that of bare C-TiO$_2$ NPs (0.5594 h^{-1}), and even faster than that of C-TiO$_2$/0.1% µGR (0.8118 h^{-1}). Fig. S7A and B showed results of the phenol photodegradation as a function of the amount of nGR and µGR. In both cases of nGR and µGR incorporation, their amount was optimized to 0.1%. It shows that a small amount of nGR and µGR leads to an effective transfer of the photogenerated charges to the separated active sites on the surface of photocatalysts. In particular, larger interfacial contact area of nGR@C-TiO$_2$ significantly decreases the number of surface defect sites such as dangling bonds, which can be attributed to the chemical bonding between the specific sites of carbon and Ti on the surface [29–32]. Too excess amount of reduced graphene oxide, however, disturbs the light absorption of the photocatalyst as well as the vertical charge-transfer. Even though the carbon sp^2 network of single and bilayer graphene exhibits unique 2D electronic transport, the mobility of electrons is not excellent along the interlayer of graphene due to the relatively weak bonding of one layer to the adjacent layer [33,34].

In order to measure the interfacial charge-transfer rate, we carried out time-resolved photoluminescence (TRPL) experiments
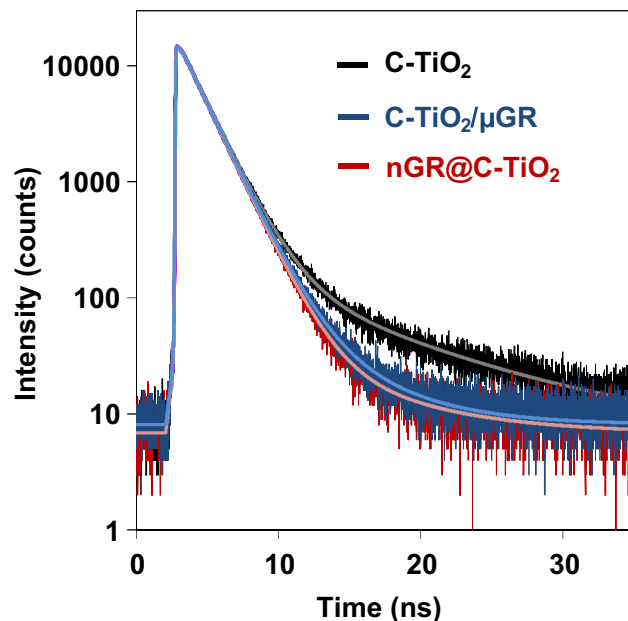

Fig. 6. Time-resolved photoluminescence spectra of 1 µM rhodamine B (RhB) in the presence of bare C-TiO$_2$ NPs, 0.1% nGR@C-TiO$_2$ and C-TiO$_2$/0.1% µGR. The fitting results (solid curves) were also included for the comparison.

(Fig. 6). Rhodamine B (RhB) was used as an indicator dye to monitor the interfacial charge-transfer. The resulting fluorescence was analyzed and fitted with biexponential kinetics [35],

$$I(t) = A_1 e^{-t/\tau_1} + A_2 e^{-t/\tau_2} \qquad (2)$$

which contains two lifetimes (τ_1 and τ_2), and the corresponding amplitudes (A_1 and A_2). The lifetime provides information on the quenching behavior. When electron transfer from RhB to adjacent
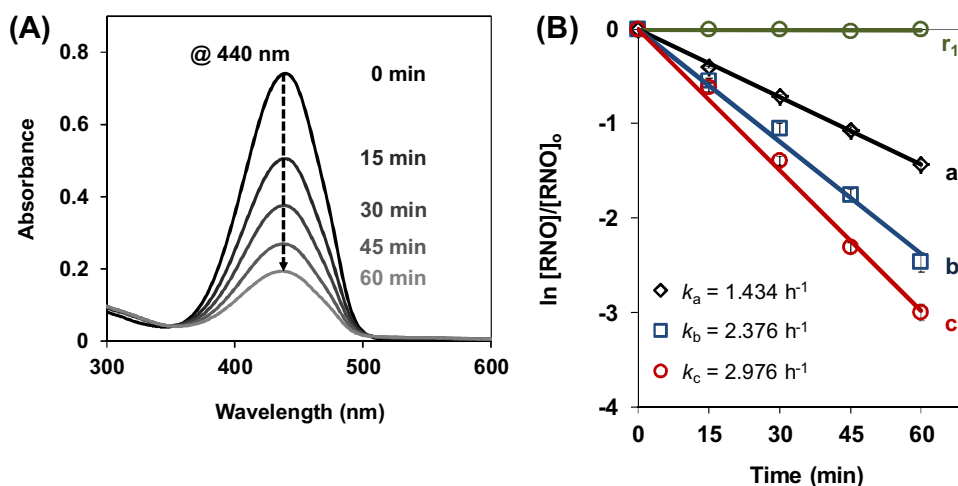
Fig. 7. (A) Time profile of p-nitrosodimethylaniline (RNO) absorbance spectrum observed in the presence of C-TiO$_2$ NPs under visible light irradiation ($\lambda \geq 420$ nm). Hydroxyl radicals ($^\bullet$OH) generation, RNO degradation, was estimated at 440 nm. (B) The observed degradation rate constant for RNO, rate constant of $^\bullet$OH formation ($k_{\bullet OH}$), was obtained from the slope of the semi-log plot for the RNO degradation. The rate constants were (a) 1.434 h^{-1} for C-TiO$_2$ NPs, (b) 2.376 h^{-1} for C-TiO$_2$/0.1% µGR, (c) 2.976 h^{-1} for 0.1% nGR@C-TiO$_2$. Any $^\bullet$OH was not generated in the presence of RNO only as a reference (r$_1$).
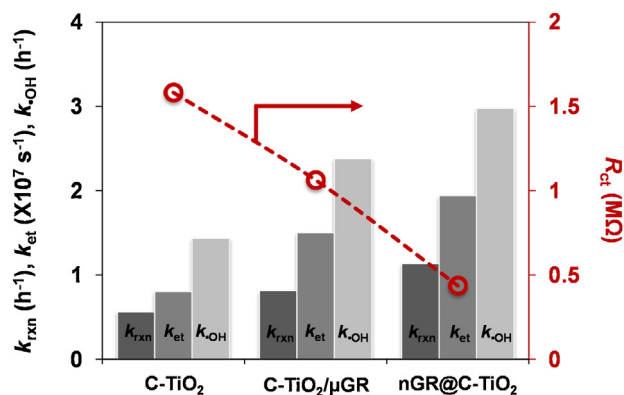
Fig. 8. Correlations of the rate constant of phenol photodegradation (k_{rxn}), electron-transfer rate constant (k_{et}), rate constant of hydroxyl radical formation ($k_{\cdot OH}$) and charge-transfer resistance (R_{ct}). The weight ratio of nGO and μGR was 0.1 wt% of C-TiO$_2$ NPs. All values were obtained under visible light irradiation ($\lambda \geq 420$ nm).

material (x) is the dominant process, it allows one to calculate the electron-transfer rate constant (k_{et}) from the emission lifetime using following equation [36,37],

$$k_{et}(\text{RhB} \to x) = \frac{1}{\tau_{\text{RhB} \to x}} - \frac{1}{\tau_{\text{RhB}}} \tag{3}$$

where RhB $\to x$ indicates the emission quenching of RhB to x. The quality of fitting was assessed by the reduced χ^2 value. Parameters and kinetics analysis of emission decay for RhB in the presence of bare C-TiO$_2$ NPs, 0.1% nGR@C-TiO$_2$ and C-TiO$_2$/0.1% μGR are summarized in Table 2. The fluorescence of an aqueous solution of pure RhB showed a monoexponential decay with an emission lifetime of 1.696 ns. The lifetime for RhB in the presence of 0.1% nGR@C-TiO$_2$ was 1.642 ns, which is faster than that of bare C-TiO$_2$ NPs (1.673 ns) and even faster than that of C-TiO$_2$/0.1% μGR (1.654 ns). The k_{et} corresponding to 0.1% nGR@C-TiO$_2$ was estimated to be 1.94×10^7 s^{-1}, and it is 2.4 times faster than that of bare C-TiO$_2$ NPs (8.04×10^6 s^{-1}). This phenomenon indicates that both case of nGR and μGR incorporation in C-TiO$_2$ NPs can inhibit the charge recombination. The nGR particularly facilitates interfacial charge-transfer from RhB to C-TiO$_2$ NPs as compared to μGR. As a result, prolonged lifetime of photogenerated charges over the C-TiO$_2$ NPs caused the formation of the larger amount of $^\bullet$OH with strong oxidizing power for phenol degradation.

In order to quantify the amount of $^\bullet$OH generated by photocatalysis, a colorimetric probe-assisted spectrometric experiments were carried out under the irradiation by visible light ($\lambda \geq 420$ nm, Fig. 7A). RNO was selected as the probe compound for detecting $^\bullet$OH. The reaction of probe compound was assumed to follow pseudo-first order kinetics where the linear slope of a semi-log plot is proportional to the concentration of $^\bullet$OH (Fig. 7B) [38,39]. The rate constant of $^\bullet$OH formation ($k_{\cdot OH}$) can be measured from the slope of following equation,

$$-\ln\frac{[\text{RNO}]}{[\text{RNO}]_0} = k_{\cdot OH} t \tag{4}$$

where [RNO]$_0$ and [RNO] represent the initial and final concentration of RNO, respectively. The $k_{\cdot OH}$ of 0.1% nGR@C-TiO$_2$ (2.976 h^{-1}) are approximately twice faster than bare C-TiO$_2$ NPs (1.434 h^{-1}). Interestingly, the $k_{\cdot OH}$ is in good agreement with k_{rxn} and k_{et}. For more clarity regarding this relationship we examined the correlation between k_{rxn}, k_{et}, $k_{\cdot OH}$ and R_{ct}. The results are presented in Fig. 8. The larger interfacial contact area of nGR@C-TiO$_2$ significantly decreases the number of surface defect sites of C-TiO$_2$ photocatalyst, which can not only reduce the interfacial resistance between C-TiO$_2$ and reactant, but form the lager amount of $^\bullet$OH.

Consequently, 0.1% nGR@C-TiO$_2$ leads to high performance in the photocatalytic degradation of phenol.

4. Conclusion

In summary, we successfully prepared the sample of C-TiO$_2$ NPs wrapped with nGR for the use as an efficient visible light responsive nano-photocatalytic material. After quantitative analyses, it is concluded that photogenerated electrons can be effectively transferred to surface active sites due to the low interfacial charge-transfer resistance between C-TiO$_2$ and reactant. As a result, prolonged lifetime of photogenerated charges over the C-TiO$_2$ NPs caused the formation of the larger amount of $^\bullet$OH with strong oxidizing power for the phenol degradation. 0.1% nGR@C-TiO$_2$ showed a particularly superior oxidative performance, which was outstanding than those of anatase TiO$_2$ NPs, P25 and bare C-TiO$_2$ NPs under irradiation by visible light. The findings from the present study show the new prospect for designing an efficient visible light responsive nano-photocatalytic material. Further investigations aimed at improving photocatalytic performance and the exploration of potential applications is currently in progress.

Appendix A. Supplementary data

Supplementary data associated with this article can be found, in the online version, at http://dx.doi.org/10.1016/j.apcatb.2013.08.030.

References

[1] J.S. Lee, K.H. You, C.B. Park, Adv. Mater. 24 (2012) 1084–1088.
[2] H. Kim, G. Moon, D. Monllor-Satoca, Y. Park, W. Choi, J. Phys. Chem. C 116 (2012) 1535–1543.
[3] Y. Zhang, Z.-R. Tang, X. Fu, Y.-J. Xu, ACS Nano 5 (2011) 7426–7435.
[4] X.-J. Lv, W.-F. Fu, C.-Y. Hu, Y. Chen, W.-B. Zhou, RSC Adv. 3 (2013) 1753–1757.
[5] Y.T. Liang, B.K. Vijayan, K.A. Gray, M.C. Hersam, Nano Lett. 11 (2011) 2865–2870.
[6] Y. Zhang, N. Zhang, Z.-R. Tang, Y.-J. Xu, Phys. Chem. Chem. Phys. 14 (2012) 9167–9175.
[7] Y. Zhang, Z.-R. Tang, X. Fu, Y.-J. Xu, ACS Nano 4 (2010) 7303–7314.
[8] H. Zhang, X. Lv, Y. Li, Y. Wang, J. Li, ACS Nano 4 (2010) 380–386.
[9] X. Wang, L. Zhi, K. Müllen, Nano Lett. 8 (2008) 237–323.
[10] H. Tong, S. Ouyang, Y. Bi, N. Umezawa, M. Oshikiri, J. Ye, Adv. Mater. 24 (2012) 229–251.
[11] M.R. Hoffmann, S.T. Martin, W. Choi, D.W. Bahnemann, Chem. Rev. 95 (1995) 69–96.
[12] A.K. Rumaiz, J.C. Woicik, E. Cockayne, H.Y. Lin, G.H. Jaffari, S.I. Shah, Appl. Phys. Lett. 95 (2009) 262111–262113.
[13] C.D. Valentin, G. Pacchioni, A. Selloni, S. Livraghi, E. Giamello, J. Phys. Chem. B 109 (2005) 11414–11419.
[14] S. Livraghi, M.C. Paganini, E. Giamello, A. Selloni, C.D. Valentin, G. Pacchioni, J. Am. Chem. Soc. 128 (2006) 15666–15671.
[15] M. Batzill, E.H. Morales, U. Diebold, Phys. Rev. Lett. 96 (2006) 026103–026106.
[16] H.J. Yun, H. Lee, J.B. Joo, N.D. Kim, J. Yi, Electrochem. Commun. 12 (2010) 769–772.
[17] X. Sun, Z. Liu, K. Welsher, J.T. Robinson, A. Goodwin, S. Zaric, H. Dai, Nano Res. 1 (2008) 203–212.
[18] D.C. Marcano, D.V. Kosynkin, J.M. Berlin, A. Sinitskii, Z. Sun, A. Slesarev, L.B. Alemany, W. Lu, J.M. Tour, ACS Nano 4 (2010) 4806–4814.
[19] H.J. Yun, H. Lee, J.B. Joo, N.D. Kim, M.Y. Kang, J. Yi, Appl. Catal. B: Environ. 94 (2010) 241–247.
[20] F. Farges, G.E. Brown Jr., J.J. Rehr, Phys. Rev. B 56 (1997) 1809–1819.
[21] V. Schwartz, D.R. Mullins, W. Yan, H. Zhu, S. Dai, S.H. Overbury, J. Phys. Chem. C 111 (2007) 17322–17332.
[22] C.D. Valentin, G. Pacchioni, A. Selloni, Chem. Mater. 17 (2005) 6656–6665.
[23] Y. Park, W. Kim, H. Park, T. Tachikawa, T. Majima, W. Choi, Appl. Catal. B: Environ. 91 (2009) 355–361.

[24] R. Fu, N. Yoshizawa, M.S. Dresselhaus, G. Dresselhaus, J.H. Satcher Jr., T.F. Baumann, Langmuir 18 (2002) 10100–10104.
[25] G. Williams, B. Seger, P.V. Kamat, ACS Nano 2 (2008) 1487–1491.
[26] H.J. Yun, H. Lee, N.D. Kim, D.M. Lee, S. Yu, J. Yi, ACS Nano 5 (2011) 4084–4090.
[27] E. Barsoukov, J.R. Macdonald, Impedance Spectroscopy, second ed., Wiley-Interscience, New York, 2005.
[28] H.J. Yun, H. Lee, J.B. Joo, W. Kim, J. Yi, J. Phys. Chem. C 113 (2009) 3050–3055.
[29] K. Woan, G. Pyrgiotakis, W. Sigmund, Adv. Mater. 21 (2009) 2233–2239.
[30] Y. Yao, G.H. Li, S. Ciston, R.M. Lueptow, K.A. Gray, Environ. Sci. Technol. 42 (2008) 4952–4957.
[31] Y. Yu, J.C. Yu, J.-G. Yu, Y.-C. Kwok, Y.-K. Che, J.-C. Zhao, L. Ding, W.-K. Ge, P.-K. Wong, Appl. Catal. A: Gen. 289 (2005) 186–196.
[32] Y.-J. Xu, Y. Zhuang, X. Fu, J. Phys. Chem. C 114 (2010) 2669–2676.

[33] R.R. Nair, P. Blake, A.N. Grigorenko, K.S. Novoselov, T.J. Booth, T. Stauber, N.M.R. Peres, A.K. Geim, Science 320 (2008) 1308.
[34] Q. Zheng, W.H. Ip, X. Lin, N. Yousefi, K.K. Yeung, Z. Li, J.-K. Kim, ACS Nano 5 (2011) 6039–6051.
[35] J.R. Lakowicz, Principle of Fluorescence Spectroscopy, third ed., Springer, New York, 2006.
[36] Y.-C. Chen, Y.-C. Pu, Y.-J. Hsu, J. Phys. Chem. C 116 (2012) 2967–2975.
[37] T.-T. Yang, W.-T. Chen, Y.-J. Hsu, K.-H. Wei, T.-Y. Lin, T.-W. Lin, J. Phys. Chem. C 114 (2010) 11414–11420.
[38] M.E. Simonsen, J. Muff, L.R. Bennedsen, K.P. Kowalski, E.G. Søgaard, J. Photochem. Photobiol. A: Chem. 216 (2010) 244–249.
[39] J. Muff, L.R. Bennedsen, E.G. Søgaard, J. Appl. Electrochem. 41 (2011) 599–607.